To appear in the *Journal of Geophysical Research*, 2001.

The theory of magnetic connectivity in the solar corona

Vyacheslav S. Titov and Gunnar Hornig
Theoretische Physik IV, Ruhr-Universität Bochum

Pascal Démoulin
DASOP, Observatoire de Paris-Meudon

Abstract

Although the analysis of observational data indicates that quasi-separatrix layers (QSLs) of magnetic configurations have to play an important role in solar flares, the corresponding theory is only at an initial stage so far. In particular, there is still a need of a proper definition of QSLs based on a comprehensive mathematical description of magnetic connectivity. Such a definition is given here by analyzing the mapping produced by the field lines which connect photospheric areas of positive and negative magnetic polarities. It is shown that magnetic configurations may have regions, where cross-sections of magnetic flux tubes are strongly squashed by this mapping. These are the geometrical features that can be identified as the QSLs. The theory is applied to quadrupole configuration to demonstrate that it may contain two QSLs combined in a special structure called hyperbolic flux tube (HFT). Both theoretical and observational arguments indicate that the HFT is a preferred site for magnetic reconnection processes in solar flares.

1. Introduction

Investigations of coronal magnetic fields extrapolated from photospheric magnetograms show a systematic spatial correlation between the locations of energy release in solar flares and the regions of strong variation of the field line connectivity [*Mandrini et al.,* 1995; *Démoulin et al.,* 1997]. Such regions, called quasi-separatrix layers (QSLs), are thought to be the plausible places for the magnetic reconnection process [*Longcope and Strauss,* 1994; *Priest and Démoulin,* 1995].

In most of the coronal volume the quasi-static conditions are fulfilled, so that the magnetic field evolves through a sequence of force-free equilibriums. These conditions, however, may easily break down in QSLs, where due to a strong variation of the field line connectivity the rearrangement of the field lines during the evolution of the configuration may occur faster than in other places. This in turn implies a locally large acceleration of plasma and hence a locally unbalanced Lorentz force, which requires the corresponding enhancement of the current density in QSLs. The importance of inertia in the current layers at the QSLs also follows from exact solutions of linearized MHD equations describing a quasi-static evolution of inhomogeneous magnetic fields [*Inverarity and Titov,* 1997].

The paper is organized as follows. In Section 2 the difference between separatrix surfaces and QSLs is discussed together with a first definition of QSLs. Section 3 describes local geometrical properties of the magnetic connectivity and gives the correct definition of QSL. Section 4 illustrates the developed theory by applying it to quadrupole magnetic configuration relevant to solar flares. The conclusions are summarized in Section 5.

2. Field line mapping

The magnetic field lines in solar active regions normally connect domains of positive and negative polarity of the photospheric plane. Choose the coordinate system, so that this plane is given by $z = 0$. The location of field line footpoints on the photosphere can be represented depending on the polarity by the radius-vector $\mathbf{r}_+ = (x_+, y_+)$ or $\mathbf{r}_- = (x_-, y_-)$. The connections of the footpoints by field lines determine two mutually inverse mappings ${}_{+}^{-}\Pi : \mathbf{r}_+ \mapsto \mathbf{r}_-$ and ${}_{-}^{+}\Pi : \mathbf{r}_- \mapsto \mathbf{r}_+$ (Figure 1). We shall simply use Π if we refer to aspects valid for both mappings. Also the representation in coordinates ${}_{+}^{-}\Pi\,(\mathbf{r}_+) \equiv (X_-(\mathbf{r}_+), Y_-(\mathbf{r}_+))$ and ${}_{-}^{+}\Pi\,(\mathbf{r}_-) \equiv (X_+(\mathbf{r}_-), Y_+(\mathbf{r}_-))$ will be used for the mappings further on.

The mapping Π is discontinuous at the footpoints of the field lines threading magnetic nulls in the corona or touching the photosphere, since the magnetic flux tubes enclosing such field lines are split at the nulls or at the so-called 'bald patches' [*Seehafer,* 1986; *Titov et al.,* 1993]. The latter are segments of the photospheric inversion line, where coronal field lines touch the photosphere. The corresponding discontinuities serve as indicators for the separatrix field lines and surfaces. It is worth to emphasize that the coordinates $(x_\pm, y_\pm)$ in this case need not to be Cartesian because the discontinuities are revealed in any system of coordinates irrespective of the metric.

However, with the help of the metric or Cartesian coordinates one can determine not only the genuine separatrices but also the QSLs. The integrity of the flux tubes is preserved within the QSLs and so the mapping Π remains continuous at the corresponding footpoints, but the shape of their cross-sections strongly changes along the flux tubes. Thus, instead of true discontinuities in Π at the intersection of the genuine separatrices with the photosphere, there are continuous but rapid variations in Π at the photospheric cross-sections of QSLs. These variations can be detected with the help of the metric only, which enables us to measure and compare the distances between the footpoints in one polarity and corresponding footpoints in the other polarity. In this respect QSLs and separatrices are qualitatively different objects. Indeed, ignoring the above metrical information about Π and using a proper continuous change of coordinates, it is possible to eliminate the rapid variations in Π and thereby the QSLs themselves, while discontinuities of Π and hence the corresponding separatrices are not removable in this way. However, as we will see the discontinuities can be considered as degenerated cases of QSLs which suggests that such QSLs must be as important as a genuine separatrix surfaces.

For the determination of the QSLs *Priest and Démoulin* [1995] proposed to use the function (called 'the norm') $N(\mathbf{r}_+)$ or $N(\mathbf{r}_-)$, which in Cartesian coordinates are

$$N(\mathbf{r}_\pm) = \left[\left(\frac{\partial X_\mp}{\partial x_\pm}\right)^2 + \left(\frac{\partial X_\mp}{\partial y_\pm}\right)^2 + \left(\frac{\partial Y_\mp}{\partial x_\pm}\right)^2 + \left(\frac{\partial Y_\mp}{\partial y_\pm}\right)^2\right]^{1/2} \equiv N_\pm\,. \quad (1)$$

It was proposed that $N(\mathbf{r}_\pm) \gg 1$ defines field lines belonging to QSLs. Yet this norm in application to different footpoints of the same field line yields generally different values N_+ and N_-, which leads to an ambiguity in the determination of QSLs. This disadvantage of the norm indicates that the adequate measure for QSLs must be invariant to the choice of the mapping ${}_+^-\Pi$ or ${}_-^+\Pi$. In the next section we find such a measure by analyzing geometrical properties of the field line connectivity.

3. Geometrical description of magnetic connectivity

3.1. Diagonalisation of the Jacobian matrix

The mapping ${}_+^-\Pi$ or ${}_-^+\Pi$ is locally described by its differential $\mathrm{d}{}_+^-\Pi$ or $\mathrm{d}{}_-^+\Pi$, respectively, which is a linear mapping from the plane tangent to the photosphere at one footpoint to a similar plane at the other footpoint. These differentials are represented by the corresponding, mutually inverse, Jacobian matrices

$$ {}_+^-\mathcal{D} = \begin{pmatrix} \frac{\partial X_-}{\partial x_+} & \frac{\partial X_-}{\partial y_+} \\ \frac{\partial Y_-}{\partial x_+} & \frac{\partial Y_-}{\partial y_+} \end{pmatrix} \equiv \begin{pmatrix} a & b \\ c & d \end{pmatrix} \qquad (2) $$

and

$$ {}_-^+\mathcal{D} = \begin{pmatrix} \frac{\partial X_+}{\partial x_-} & \frac{\partial X_+}{\partial y_-} \\ \frac{\partial Y_+}{\partial x_-} & \frac{\partial Y_+}{\partial y_-} \end{pmatrix} = \Delta_+^{-1} \begin{pmatrix} d & -b \\ -c & a \end{pmatrix}, \qquad (3) $$

$$ \Delta_+ = ad - bc \equiv \det {}_+^-\mathcal{D}. \qquad (4) $$

We assume hereafter that $(x_\pm, y_\pm)$ are measured in one Cartesian system of coordinates covering the whole photospheric plane. Equations (2) and (3) show that it is sufficient to have only one of these matrices for a local description of the magnetic connectivity.

The determinant Δ_+ is always negative in the chosen coordinate system. This can easily be seen for the simplest arcade-like magnetic configuration, which is symmetric about its photospheric inversion line $y = 0$ separating positive and negative polarities at the upper ($y > 0$) and lower ($y < 0$) half planes, respectively. Due to the assumed symmetry $X_-(x_+, y_+) \equiv x_+$ and $Y_-(x_+, y_+) \equiv -y_+$, so that $a = 1$, $b = 0$, $c = 0$ and $d = -1$, which in turn yields $\Delta_+ = -1$. Any other configuration with the same trivial topology can be obtained from the considered one by using a suitable smooth deformation. Such a deformation generally changes the absolute value of Δ_+, but preserves its sign, so that Δ_+ always has to be negative.

The negative sign of Δ_+ is related with the reversing of the orientation of the vector basis by the $\mathrm{d}{}_+^-\Pi$-mapping. Indeed, let us take in the tangent plane at some footpoint $\mathbf{r}_+$ an orthonormal vector basis $(\hat{\mathbf{u}}_+, \hat{\mathbf{v}}_+)$ having a right-handed orientation, which means that $\hat{\mathbf{u}}_+ \times \hat{\mathbf{v}}_+ \cdot \hat{\mathbf{z}} = 1$, where $\hat{\mathbf{z}}$ is a unit vector along z-axis. This basis is generally mapped by $\mathrm{d}{}_+^-\Pi$ into a non-orthonormal basis $(\mathbf{u}_-, \mathbf{v}_-)$ in the corresponding tangent plane at ${}_+^-\Pi(\mathbf{r}_+)$ by giving $\mathbf{u}_- \times \mathbf{v}_- \cdot \hat{\mathbf{z}} = \Delta_+ < 0$. Thus the basis $(\mathbf{u}_-, \mathbf{v}_-)$ must have the left-handed orientation (Figure 2a).

The angle between $\mathbf{u}_-$ and $\mathbf{v}_-$ depends not only on the matrix ${}_+^-\mathcal{D}$ but also on the orientation of the orthonormal basis $(\hat{\mathbf{u}}_+, \hat{\mathbf{v}}_+)$. It turns out that by rotating the latter one can yield an orthogonal pair $(\mathbf{u}_-, \mathbf{v}_-)$ (Figure 2b). To show this we use angles γ_+ and γ_- which determine the directions of $\hat{\mathbf{u}}_+$ and $\mathbf{u}_-$ with respect to the x-axis and corresponding matrices of rotations of these vectors $\mathcal{R}_{\gamma_+}$ and $\mathcal{R}_{\gamma_-}$. Regarding now the vectors as appropriate columns of coordinates and denoting $\hat{\mathbf{x}} = (1\ 0)^{\mathrm{T}}$ and $\hat{\mathbf{y}} = (0\ 1)^{\mathrm{T}}$, we obtain from Figure 2b that $\hat{\mathbf{u}}_+ = \mathcal{R}_{\gamma_+}\hat{\mathbf{x}}$ and $\mathbf{u}_- = \lambda_1 \mathcal{R}_{\gamma_-}\hat{\mathbf{x}}$, where $\lambda_1 \equiv |\mathbf{u}_-|$. By definition, however, $\mathbf{u}_- = {}_+^-\mathcal{D}\,\hat{\mathbf{u}}_+$ and therefore $\mathcal{R}_{\gamma_-}^{-1}\,{}_+^-\mathcal{D}\,\mathcal{R}_{\gamma_+}\hat{\mathbf{x}} = \lambda_1\,\hat{\mathbf{x}}$.

Similarly, $\hat{\mathbf{v}}_+ = \mathcal{R}_{\gamma_+}\hat{\mathbf{y}}$ and $\mathbf{v}_- = {}_+^-\mathcal{D}\hat{\mathbf{v}}_+$, result in $\mathbf{v}_- = {}_+^-\mathcal{D}\mathcal{R}_{\gamma_+}\hat{\mathbf{y}}$. To satisfy the condition $\mathbf{u}_- \perp \mathbf{v}_-$ we have to require $\mathbf{v}_- = \lambda_2 \mathcal{R}_{\gamma_-}\hat{\mathbf{y}}$, where $\lambda_2 \equiv -|\mathbf{v}_-|$ is negative because $\mathrm{d}{}_+^-\Pi$ reverses the orientation of the basis. Thus both $\hat{\mathbf{y}}$ and $\hat{\mathbf{x}}$ are eigenvectors of the same matrix $\mathcal{R}_{\gamma_-}^{-1}\,{}_+^-\mathcal{D}\,\mathcal{R}_{\gamma_+}$. Summarizing all these calculations as

$$ \mathcal{R}_{\gamma_-}^{-1}\,{}_+^-\mathcal{D}\,\mathcal{R}_{\gamma_+} = \mathrm{diag}(\lambda_1, \lambda_2) \equiv \Lambda, \qquad (5) $$

we see that the condition $\mathbf{u}_- \perp \mathbf{v}_-$ requires that the two non-diagonal elements of $\mathcal{R}_{\gamma_-}^{-1}\,{}_+^-\mathcal{D}\,\mathcal{R}_{\gamma_+}$ must vanish. For a given matrix ${}_+^-\mathcal{D}$ these requirements determine the angles γ_+ and γ_-. The calculation of the angles is facilitated significantly if we introduce the following complex variables ($\mathrm{i} = \sqrt{-1}$)

$$ \xi = a + d + \mathrm{i}\,(b - c), \qquad (6) $$

$$ \zeta = a - d + \mathrm{i}\,(b + c). \qquad (7) $$

Expressing a, b, c and d from (6) and (7) in terms of $|\xi|$, $\arg\xi$, $|\zeta|$, $\arg\zeta$ and then substituting them into (5), one obtains after some transformations

$$ \Lambda = \begin{pmatrix} \frac{|\xi|\cos\alpha + |\zeta|\cos\beta}{2} & -\frac{|\xi|\sin\alpha + |\zeta|\sin\beta}{2} \\ \frac{|\xi|\sin\alpha - |\zeta|\sin\beta}{2} & \frac{|\xi|\cos\alpha - |\zeta|\cos\beta}{2} \end{pmatrix}, \qquad (8) $$

where

$$ \alpha = \gamma_+ - \gamma_- - \arg\xi, \qquad (9) $$

$$ \beta = \gamma_+ + \gamma_- - \arg\zeta. \qquad (10) $$

The matrix Λ is diagonal and hence the basis $(\mathbf{u}_-, \mathbf{v}_-)$ is orthogonal if $\alpha = \beta = 0$, which yields

$$\gamma_+ = (\arg\xi + \arg\zeta)/2, \quad (11)$$
$$\gamma_- = (\arg\zeta - \arg\xi)/2. \quad (12)$$

The diagonal elements of (8) in this case simply become

$$\lambda_1 = (|\xi| + |\zeta|)/2, \quad (13)$$
$$\lambda_2 = (|\xi| - |\zeta|)/2. \quad (14)$$

Other solutions with $\alpha = \pi$ and/or $\beta = \pi$ are also possible but not of interest, since they are the result of mirror reflections about the directions given by (11) and (12).

By using (13) and (14) together with (7),(6),(1) and (2) one obtains

$$|\mathbf{u}_- + \mathbf{v}_-| = (a^2 + b^2 + c^2 + d^2)^{1/2} \equiv N_+. \quad (15)$$

Thus the norm N_+ determines simply the length of the diagonal in the rectangular constructed on the orthogonal vectors $\mathbf{u}_-$ and $\mathbf{v}_-$ (Figure 2b).

3.2. The degree of squashing

Let us determine similar characteristics for the reverse differential $\mathrm{d}\underline{\underline{\Pi}}_+$ at $\mathbf{r}_- = {}_+\underline{\underline{\Pi}}_-(\mathbf{r}_+)$. The simplest way to do this is just to change in (11)–(14) the superscripts $\pm$ on $\mp$ and the elements of ${}_+\underline{\underline{\mathcal{D}}}_-$ (2) to the corresponding elements of $\underline{\underline{\mathcal{D}}}_+$ (3). Then we obtain for the complex values similar to (6) and (7)

$$\tilde{\xi} = [d + a - \mathrm{i}\,(b - c)]/\Delta_+ \equiv \bar{\xi}/\Delta_+, \quad (16)$$
$$\tilde{\zeta} = [d - a - \mathrm{i}\,(b + c)]/\Delta_+ \equiv -\zeta/\Delta_+, \quad (17)$$

yielding the following angles:

$$\tilde{\gamma}_+ = (\arg\xi + \arg\zeta + \pi)/2 = \gamma_+ + \pi/2, \quad (18)$$
$$\tilde{\gamma}_- = (\arg\zeta - \arg\xi + \pi)/2 = \gamma_- + \pi/2. \quad (19)$$

They show that the orthonormal basis $(\hat{\mathbf{u}}_-, \hat{\mathbf{v}}_-)$ corresponding to this solution is rotated by $\pi/2$ with respect to the basis $(\mathbf{u}_-, \mathbf{v}_-)$ and the same is valid for $(\mathbf{u}_+, \mathbf{v}_+)$ and $(\hat{\mathbf{u}}_+, \hat{\mathbf{v}}_+)$ (Figure 2b, c). Defining $\tilde{\lambda}_1$ and $\tilde{\lambda}_2$ in analogy to (13) and (14) and using $\Delta_+ = \lambda_1\lambda_2$ together with (16) and (17) we obtain

$$\tilde{\lambda}_1 = -1/\lambda_2, \quad (20)$$
$$\tilde{\lambda}_2 = -1/\lambda_1. \quad (21)$$

So the norm in the negative polarity at the footpoint $\mathbf{r}_- = {}_+\underline{\underline{\Pi}}_-(\mathbf{r}_+)$ is

$$N_- \circ {}_+\underline{\underline{\Pi}}_- = N_+/|\Delta_+|, \quad (22)$$

hereafter the symbol $\circ$ stands for the composition of the corresponding functions.

This consideration shows that the determination of QSLs by means of the norms N_+ and N_- must really lead to different results if $|\Delta_+| \neq 1$. For example, consider the potential configuration, in which a small photospheric area of concentrated positive flux is surrounded by a large negative polarity with the same absolute value of the flux. This configuration can be modeled by fictive positive and negative charges, which are equal in absolute value and placed below the photosphere on different depths l and L, respectively, such that $l \ll L$. Field lines 'fountain' here from the positive to the negative polarity, so that $N_+ \gg 1$ and $N_- \ll 1$. Thus, we have a contradictory case, where being applied to different polarities the norm yields different results.

One could try to avoid this ambiguity by requiring that *both* conditions $N_+ \gg 1$ and $N_- \gg 1$ should be satisfied in QSLs. According to (22) this would actually be equivalent to finding regions in the positive polarity, where both $N_+ \gg 1$ and $N_+/|\Delta_+| \gg 1$ are fulfilled. In principle, nothing is wrong here accept that the description of QSLs simultaneously by two different functions does not look like a well-founded approach.

Alternatively, one could sacrifice the symmetry of the QSL definition with respect to the 'positive' and 'negative' footpoints by requiring that N_+ *or* N_- must be large in QSLs. Then the configurations like the one in the above example would be identified as QSLs. However, they show no connection to any true separatrix surface in whatsoever limiting case, thus such a criterion of QSL should also be discarded.

The described difficulty may be resolved in the following way. Notice first that the mapping Π can locally be described by λ_1, λ_2, γ_+ and γ_-. Here only λ_1 and λ_2 determine the value of footpoint displacements, while γ_+ and γ_- define their directions. So it would be natural if the required characteristics is a function of λ_1 and λ_2 only. Let us show that this is actually the ratio $|\lambda_1/\lambda_2|$. According to (20) and (21) (see also Figure 2b, c) it coincides with the ratio $|\tilde{\lambda}_1/\tilde{\lambda}_2|$ and thereby characterizes the magnetic connectivity itself rather than one of the mappings ${}_+\underline{\underline{\Pi}}_-$ or $\underline{\underline{\Pi}}_+$. If we define the elemental flux tubes (EFTs) as tubes with infinitesimal cross-sections, then $|\lambda_1/\lambda_2|$ determines the degree of squashing of the EFTs at their photospheric ends (see shaded regions in Figure 2b, c). Normally this quantity has to be of the order of unity and only in special regions it may become

extremely large. By using (6)–(14) one can derive that

$$|\lambda_1/\lambda_2| = Q/2 + \sqrt{Q^2/4 - 1}, \quad (23)$$

$$Q = N_+^2/|\Delta_+|, \quad (24)$$

which shows that $|\lambda_1/\lambda_2| \approx Q$ for $Q \gg 1$. Q can be interpreted geometrically with the help of the rectangle built on the vectors $\mathbf{u}_-$ and $\mathbf{v}_-$ (see Figure 2b) as the ratio of its diagonal squared to its area, because $|\Delta_+| = |\mathbf{u}_-|\,|\mathbf{v}_-|$. This means also that $Q = (\lambda_1^2 + \lambda_2^2)/|\lambda_1\lambda_2|$ and so $\min Q = 2$ at $|\lambda_1| = |\lambda_2|$. The expression for Q has an elegant form, invariant to interchanging of $+$ and $-$, and simpler than (23), so it is reasonable to define that

> *the QSL is a layer-like flux tube consisting of magnetic field lines with* $Q \gg 2$.

Bearing in mind the above mentioned properties of Q, one can call this quantity *QSL squashing degree*. Equation (24) implies that the QSLs defined with the help of Q or N_+ have to be essentially different if the determinant Δ_+ varies in the photospheric plane as strong as N_+.

Here it is worth mentioning a related quantity, namely the so-called differential flux volume

$$V(\mathbf{r}_+) = \int_{\mathbf{r}_+}^{{}_+\Pi_-(\mathbf{r}_+)} \frac{\mathrm{d}l}{B} \equiv V({}_+\Pi_-(\mathbf{r}_+)), \quad (25)$$

in which the integration is carried out along the corresponding field line. It defines the ratio of volume and magnetic flux of an elemental flux tube enclosing a given field line, since

$$V(\mathbf{r}_+) = \int_{\mathbf{r}_+}^{{}_+\Pi_-(\mathbf{r}_+)} \frac{\delta S}{\delta\Phi}\mathrm{d}l = \frac{1}{\delta\Phi}\int_{\mathbf{r}_+}^{{}_+\Pi_-(\mathbf{r}_+)} \delta S\,\mathrm{d}l,$$

where δS and $\delta\Phi \equiv B\delta S$ are the cross-section of that tube and magnetic flux in it, respectively. This value has appeared in the analysis of current sheet formations along separatrix surfaces in quasi-static evolutions of $2\frac{1}{2}$D magnetic configurations [*Zwingmann et al.,* 1985; *Low and Wolfson,* 1988; *Vekstein et al.,* 1991; *Vekstein and Priest,* 1992]. It has also been used (under the name 'delay function') for studying 3D magnetic topology caused by the presence of null points [*Lau,* 1993]. Recently *Schindler and Birn* [1999] have shown that strong spatial variations of V may cause a similar formation of current layers in 3D magnetic fields. So at first sight it seems natural to use this value for characterizing QSLs. However, one can see from the definition of V that it *depends* not only on the field line connections of the points in different polarities but *also on the field line properties in the coronal volume.* Therefore, V is not a measure for the field line connectivity alone. For example, if one fixes the foot points of the field lines in a given configuration and exposes the coronal volume to a smooth deformation, then V will change in response to such a deformation, while the field line connectivity will remain the same. Thus, V cannot be used as a measure of the connectivity, which does not reduce, however, its value in understanding the process of current sheet formation, because this process may depend not only on the connectivity but on other factors as well (see also Section 4.3).

3.3. Expansion-contraction degree

The QSL-squashing degree Q provides the most important information about the magnetic connectivity. However, it is only a part of the whole information provided by the Jacobian matrix, which has four independent parameters. The second characteristic of the connectivity can be obtained as follows. Since ${}_+\Pi_-$ and ${}_-\Pi_+$ are mutually inverse mappings (see also (3) and (4)), the quantities $|\Delta_+|$ and $|\Delta_-|^{-1}$ ($\equiv |\det \mathcal{D}_+|^{-1}$) have the same value if they are evaluated at the corresponding footpoints of a given field line. In other words,

$$K \equiv \lg|\Delta_+| \equiv -\lg|\Delta_- \circ {}_+\Pi_-| \quad (26)$$

and so $|K|$ is invariant to an interchange of $+$ and $-$. Therefore $|K|$ can be used as a second independent characteristic of the magnetic connectivity.

However, the sign of K yields an extra information, which shows whether an EFT (elemental flux tube) starting at the point of the evaluation expands ($K > 0$) or contracts ($K < 0$) towards its other footpoint. If one plots the distribution of K together with the photospheric inversion line separating positive and negative polarities, it will show not only the degree of expansion of EFTs, but also the direction in which this expansion occurs. Thus, for characterizing magnetic connectivity it is better to use the value K than its modulus. Further K will be called *the expansion-contraction degree* of EFTs.

The conservation of magnetic flux in flux tubes enables us to express K in terms of the normal component of the photospheric magnetic field. Indeed, let an EFT have the cross-section $|\delta x_+ \delta y_+|$ in the positive polarity, then the equality of magnetic flux

at the ends of the EFT means that $|B_{z+}\,\delta x_+\delta y_+| = |B_{z-}\circ {}_+\underline{\Pi}_-\,\Delta_+\delta x_+\delta y_+|$, where $B_{z+}\equiv B_z(x_+,y_+,0)$ and $B_{z-}\equiv B_z(x_-,y_-,0)$ are normal components of the magnetic field in the corresponding polarities. Therefore for the positive polarity we have

$$K = \lg\left|\frac{B_{z+}}{B_{z-}\circ {}_+\underline{\Pi}_-}\right|, \tag{27}$$

while the interchange of $+$ and $-$ in this formula determines K for the negative polarity. Here we used that Jacobian of the field line mapping coincides with the ratio of B_z-components at the ends of field lines. This ratio is much easier to compute than the Jacobian, so that formula (27) is more valuable for application than (26). Also it is a bit more convenient to plot this ratio in a logarithmic scale rather than K itself.

3.4. Orthogonal parquet

One can see from (18) and (19) that $\gamma_+ - \gamma_-$ and any π-periodic function of $\gamma_+ + \gamma_-$ are also invariant with respect to the direction of mapping Π. Being independent on Q and K, these invariants could additionally be used for characterizing magnetic connectivity. Unfortunately, their plots are not much meaningful for the interpretation compared to Q and K. This motivated us to use these angles for obtaining a more transparent graphical representation.

Remember that (see Section 3.1) γ_+ and γ_- determine at the footpoints of a given field line the orientations at which the orthogonal vector bases are mapped into each other. This defines two mutually orthogonal vector fields on the photosphere. The integral lines of both fields intersect each other orthogonally and thus form what we call *the orthogonal parquet*. In the positive polarity the lines with tangents inclined at the angles γ_+ correspond to the dilation coefficient λ_1, while the lines orthogonal to them correspond to λ_2. In the negative polarity the lines with tangents inclined at the angles γ_- correspond to the dilation coefficient $\tilde\lambda_1$, while the lines orthogonal to them correspond to $\tilde\lambda_2$. The corresponding tiles of the parquet are interconnected by Π, so that (20) and (21) are fulfilled. Thus, such a parquet visualizes the properties of magnetic connectivity described by γ_+ and γ_-. In fact, the properties determined by Q and K or λ_1 and λ_2 can also be incorporated in the parquet if one chooses properly sizes of the tiles or, in other words, the proper parameterization of the integral lines.

Indeed, we can regard the whole magnetic configuration in the corona as a collection of EFTs with infinitesimal photospheric cross-sections $\sim\delta^2$. Given the rectangles $(\lambda_1^{-1/2}\delta)\times(|\lambda_2|^{-1/2}\delta)$ in the positive polarity with the first side inclined at angles γ_+ (cf. Figure 2), it follows then from (5) rewritten as

$${}_+\underline{\mathcal{D}} = \mathcal{R}_{\gamma_-}\,\Lambda\,\mathcal{R}_{\gamma_+}^{-1} \tag{28}$$

that the corresponding cross-sections in the negative polarity are also rectangles but of the size $(\lambda_1^{1/2}\delta)\times(|\lambda_2|^{1/2}\delta)$ with the first side inclined at angles γ_-.

This is actually nothing more than a construction of the orthogonal parquet in the limit of vanishing rectangular tiles ($\delta\to 0$). To describe the parquet with tiles of finite size (curvilinear rectangles now), assume that the parquet lines corresponding to λ_1 and λ_2 are determined in positive polarity by $(x_{+1}(s_1),y_{+1}(s_1))$ and $(x_{+2}(s_2),y_{+2}(s_2))$. Choose the parameters s_1 and s_2 so that their infinitesimal increments $\mathrm{d}s_1$ and $\mathrm{d}s_2$ correspond to δ in the above discussion, then the parquet lines have to satisfy

$$\frac{\mathrm{d}x_{+1}}{\mathrm{d}s_1} = \frac{\cos\gamma_+}{\sqrt{\lambda_1}}, \tag{29}$$

$$\frac{\mathrm{d}y_{+1}}{\mathrm{d}s_1} = \frac{\sin\gamma_+}{\sqrt{\lambda_1}}, \tag{30}$$

and

$$\frac{\mathrm{d}x_{+2}}{\mathrm{d}s_2} = -\frac{\sin\gamma_+}{\sqrt{|\lambda_2|}}, \tag{31}$$

$$\frac{\mathrm{d}y_{+2}}{\mathrm{d}s_2} = \frac{\cos\gamma_+}{\sqrt{|\lambda_2|}}. \tag{32}$$

The equations for the parquet in the negative polarity are obtained similarly. Hereafter the integral lines of systems (29)–(30) and (31)–(32), respectively, will be called λ_1- and λ_2-lines.

To construct the orthogonal parquet, it is necessary first to take an origin O_+ as an initial point for integrating (29)–(30) and compute the λ_1-line passing through this point. Then the points belonging to this line can be used as initial points for (31)–(32) to compute the corresponding set of λ_2-lines. The λ_2-line passing through O_+ yields in turn initial points for (29)–(30), whose integration gives the corresponding set of λ_1-lines. If the initial points in this procedure are chosen equidistantly in parameter space, namely $\Delta s_1=\delta$ and $\Delta s_2=\delta$, with a sufficiently small step δ, then the aspect ratio of the parquet tiles will be $\approx\sqrt{\lambda_1/|\lambda_2|}$ and, in particular, $\approx\sqrt{Q}$ at QSLs. Doing the same in the negative polarity with the origin

O_- mapped from O_+ by $\underset{+}{\Pi}_{-}$, one can reproduce the parquet in the whole photosphere. The ratio of tile areas interconnected by field lines will approximately coincide in this case with the corresponding local values of the Jacobian. So the orthogonal parquet gives a complete and convenient representation of magnetic connectivity.

3.5. Critical points of the parquet

The present construction of the parquet is well defined everywhere except for the points, where

$$\xi = 0. \tag{33}$$

At these points $\arg\xi$ and hence γ_+ and γ_- are not defined, so they are critical for (29)–(32). One can see from (13) and (14) that first $\lambda_1 = -\lambda_2$ and hence Q attains there its absolute minimum value 2 (see (23)). Secondly, vanishing of ζ is impossible, since it would mean that $\lambda_1 = \lambda_2$, which contradicts to that $\lambda_1\lambda_2 = \Delta_+ < 0$. Thus, the critical points are defined by (33) only. The behavior of the parquet in their vicinity requires a special consideration. It is sufficient to do this for λ_1-lines, since the properties of λ_2-lines are similar. It happens that in this case

$$\tau \equiv \tan\gamma_+$$

is more convenient for parameterizing λ_1-lines than s_1. Using this notation and (11), one can rewrite $\tan 2\gamma_+$ as

$$\frac{2\tau}{1-\tau^2} = \frac{\tan(\arg\xi) + \tan(\arg\zeta)}{1 - \tan(\arg\xi)\tan(\arg\zeta)}. \tag{34}$$

From here we are now going to derive an approximate analytic form of the λ_1-lines in the vicinity of critical points. Note first that according to (6) and (33)

$$d = -a, \tag{35}$$
$$c = b \tag{36}$$

at such points, so (7) yields

$$\tan(\arg\zeta) \approx b/a. \tag{37}$$

Keeping also the first order terms in Taylor expansion of (6) at a given critical point, we have

$$\tan(\arg\xi) \approx \frac{\xi_{Ix}\,x + \xi_{Iy}\,y}{\xi_{Rx}\,x + \xi_{Ry}\,y}, \tag{38}$$

where the indices I and R stand for the imaginary and real parts of ξ, respectively, and the indices x and y denote the corresponding derivatives at the critical point – for example, $\xi_{Ix} = \partial\Im(\xi)/\partial x) = \partial b/\partial x - \partial c/\partial x$.

By substituting (37) and (38) into (34) and making some transformations one can obtain

$$y/x = P_1(\tau)/P_2(\tau), \tag{39}$$

where

$$P_1(\tau) = (a\xi_{Ix} + b\xi_{Rx})(1-\tau^2) - 2(a\xi_{Rx} - b\xi_{Ix})\tau, \tag{40}$$
$$P_2(\tau) = (a\xi_{Iy} + b\xi_{Ry})(\tau^2-1) + 2(a\xi_{Ry} - b\xi_{Iy})\tau. \tag{41}$$

Since on λ_1-lines $\mathrm{d}y/\mathrm{d}x = \tau$, the differentiation of (39) yields the following equation for $x(\tau)$

$$\frac{\mathrm{d}\ln x}{\mathrm{d}\tau} = \frac{P_1'(\tau)P_2(\tau) - P_1(\tau)P_2'(\tau)}{P_2(\tau)(\tau P_2(\tau) - P_1(\tau))}, \tag{42}$$

which can be integrated to give

$$\frac{x}{x_0} = \frac{P_2(\tau)}{P_2(\tau_0)} \prod_{i=1}^{3} \left|\frac{\tau-\tau_i}{\tau_0-\tau_i}\right|^{k_i-1}. \tag{43}$$

Here the index 0 denotes the corresponding initial values, while τ_i are the roots of the cubic equation $P_3(\tau) = 0$ such that

$$P_3(\tau) = \tau P_2(\tau) - P_1(\tau) \tag{44}$$

and

$$k_i = P_2(\tau_i)/P_3'(\tau_i) \tag{45}$$

with the prime standing for the derivative to τ_i.

Equation (43) corresponds to the case, where all the roots τ_i are real. However, if only one of the roots, say, τ_3 is real, then the solution is

$$\frac{x}{x_0} = \frac{P_2(\tau)}{P_2(\tau_0)} \left|\frac{\tau-\tau_3}{\tau_0-\tau_3}\right|^{k_3-1} \left[\frac{(\tau-\tau_1)(\tau-\bar\tau_1)}{(\tau_0-\tau_1)(\tau_0-\bar\tau_1)}\right]^{\Re(k_1)-1} \times \exp\left\{2\Im(k_1)\left[\arg(\tau_1-\tau_0) - \arg(\tau_1-\tau)\right]\right\}. \tag{46}$$

This expression actually follows from (43) if one omits there the modulus at $i = 1, 2$.

Thus, the λ_1-lines in the vicinity of a critical point of the parquet are described in general either by (43) and (39) or by (46) and (39). In the first case there are separatrices emanating from the critical point in the directions with tangents τ_1, τ_2 and τ_3 (Figure 3a). In the second case there is a single separatrix and its tangent equals τ_3 (Figure 3b). The characteristic structure of λ_1-lines suggests to classify the critical

points in I- or Y-type depending on the number of separatrices (one or three, respectively) they have. A similar analysis of λ_2-lines shows that their local structure at a critical point is the same as for λ_1-lines but rotated on 180° around this point (Figure 3).

The structure of the orthogonal parquet breaks down at the critical points in the following way. Any *Y-point* is a vertex for *six adjoint tetragons* (Figure 3a), while a normal point is a vertex for four adjoint rectangles. Any *I-point* belongs to a common side of *two adjoint triangles* rather than rectangles in the normal case. The consideration of particular examples shows also that the separatrices emanating from these points connect the points or go to infinity. In the result the whole photospheric plane is uniquely divided by separatrices in several domains, whose corners are the critical points. Each of these domains is smoothly covered by the orthogonal parquet, while its 'defects' are localized at the critical points in the above mentioned way. Thus the critical points of the parquet describe a *global geometrical complexity* of topologically simple magnetic configurations. A more detailed investigation of the orthogonal parquet is certainly required, but it goes far beyond the scope of the present work and so we restrict ourselves here by an illustrative example (see Section 4.5).

4. Application of the theory to a quadrupole configuration

Let us see what the above formulated theory yields for the configuration formed by two bipolar groups of sunspots. Such a configuration is considered for a long time as a basic model for solar prominences [*Kippenhahn and Schlüter,* 1957] and flares [*Sweet,* 1969] and it is quite instructive for our purposes. In an idealized form the corresponding sunspots can be modeled by point-like sources $e_1, \ldots, e_4$ of potential magnetic flux. The configuration has a non-trivial topological structure due to the presence of null points in the field. This means that all separatrix surfaces here are formed by field lines emanating from the nulls. For a wide range of positions and strengths of the sources there are only two nulls N_1 and N_2 with the separatrices intersecting along a special field line called 'separator' ([*Baum and Bratenahl,* 1980], Figure 4). The same is also true for a bit more general configuration with the sources spread on the photosphere in finite regions, outside of which the vertical component of the field vanishes [*Sweet,*1969]. The neighborhood of the separator here has to be favorable for the development of a current sheet and a magnetic reconnection process. This follows from the tendency of the highly conducting solar plasma to preserve the magnetic topology of the configuration during its evolution. Therefore the presence of the nulls in the field is a crucial argument for the current sheet formation in this configuration.

4.1. Distributed versus concentrated sources

In reality, however, the vertical magnetic field is distributed on the *whole* photospheric plane. To incorporate this fact, *Gorbachev and Somov* [1988] modified the idealized configuration by placing the sources below the photosphere. The sources here become fictive in the sense that they determine a physically meaningful field only in the corona and on the photosphere but not below it, where the magnetic field is certainly not potential. This trick significantly facilitates the calculation of a potential coronal field corresponding to a rather complicated effective magnetogram (Figure 5), since the resulting field here is just a superposition of the fields produced by the fictive sources. However, such an 'innocent' modification of the model leads to serious topological consequences: the nulls determining the separator disappear from the photosphere together with the sources. This means that the separator in the form as defined above *does not exist* anymore. Therefore it is inconsistent to introduce the separator into the above realistic configuration by simply identifying it with the separator of the fictive source system, as suggested by *Gorbachev and Somov* [1988] (see Figure 6).

In fact, the coronal magnetic topology in such a case may be non-trivial only due to the field lines starting at bald patches [*Seehafer,* 1986; *Titov et al.,* 1993], and indeed, there is a substantial range of parameters for the above configuration, where this situation is realized [*Titov et al.,* 1993]. It gives *the generalized separator field line* [*Bungey et al.,* 1996], which is a limiting case of the normal one [*Titov,* 1998]. However, one can prove that for the particular example shown in Figure 5 the coronal nulls and bald patches are absent and so the configuration is topologically as simple as an arcade-like field. Thus, the self-consistent topological approach does not reveal in this case any site preferable for the reconnection process.

This negative but mathematically strict conclusion contradicts an intuitive feeling that both the idealized and realistic configurations must have similar physical properties. The discrepancy becomes even stronger if

one takes into account the success of the Gorbachev-Somov model in explaining some observed features of solar flares (see Section 4.4). This successful part of the model has been confirmed and developed later by other authors ([*Démoulin et al.,* 1997] and references therein). Nevertheless, the above discrepancy remained unresolved in these works, since they followed the erroneous paradigm that a strong variation of magnetic connectivity can be interpreted exclusively as a topological effect.

4.2. A hyperbolic flux tube (HFT)

The above discrepancy can be resolved only in the framework of a geometrical approach, which describes equally good both topological and geometrical features of magnetic connectivity [*Titov and Hornig,* 2002]. Indeed, the computation of Q-distribution for the above topologically simple field (Figure 5) reveals on the photosphere two very narrow strips with extremely high values of Q attaining $\sim 10^6$ in maximum (see Figure 7a). The distribution of $|\Delta| = |\lambda_1 \lambda_2| \equiv 10^K$ represented in logarithmic scale (Figure 7b) has a very large gradient at these strips, because they separate two extended areas (elongated light grey regions) of small $|\Delta|$ with the minimums $\sim 10^{-2}$ and end up in smaller areas (compact dark grey regions) of large $|\Delta|$ with the maximums $\sim 10^2$.

The strips here correspond to the photospheric cross-sections of a magnetic flux tube which according to our definition could be identified as a QSL. A more detailed consideration below, however, shows that it is actually worth to distinguish two QSLs in this tube. The way they appear here suggests to call such a tube a *hyperbolic flux tube* (HFT) and its photospheric cross-sections HFT-traces. The structure of the HFT becomes clear if one computes the magnetic flux surface forming its boundary. It is natural to determine such a surface by the condition $Q = \text{const} \gg 2$, in which we have chosen $Q = 100$ for the HFT under study. Other choices of Q are also possible, but they define a similar larger or smaller surface depending on whether the new Q is smaller or larger as the old one, respectively.

Figure 8 shows a rather non-trivial structure of the HFT: it starts first at each of the above mentioned strips on the photosphere as a thin layer and then quickly transforms in the corona into a tube with an X-type cross-section in the middle (see Figure 9). The behavior of the field lines on the boundary of the HFT helps to understand its basic properties. Notice first that this boundary surface intersects the photosphere at the two very stretched ovals of crescent shape. The field lines starting at the ends of one of the crescents form a narrow bunch, which diverges hyperbolically in the corona and ends up at one side of the other crescent. This remains valid for the flux surfaces characterized by larger boundary values of Q, so that such a hyperbolic structure of magnetic flux recurs inside the HFT on smaller scales. The latter seems to be a characteristic feature of the HFT motivating its name. The relationship between the HFT and QSLs will be clarified in the next subsection, where the limiting transition of the HFT to the genuine separatrices is considered.

4.2.1. Degenerate case of the HFT. Consider now what happens in our example when the fictive sub-photospheric sources appear on the photosphere. This implies that the depth of the sources $d \to 0$ and the magnetic flux distributed over the whole photosphere is concentrating in point-like sources. At each non-vanishing d the configuration has a simple arcade-like magnetic topology, while at $d = 0$ it acquires a non-trivial topological structure shown in Figure 4. To understand how the HFT evolves in this limiting process, determine the HFT-boundary with the help of $Q = Q_{\max}/2$, where $Q_{\max}$ is the corresponding maximal value of Q on the photosphere at a fixed d. It is clear that $Q_{\max} \to \infty$ at $d \to 0$, since in the limiting configuration null points appear on the photosphere. As was mentioned above, all HFTs irrespective of the boundary value of Q have a similar form shown in Figure 8.

This figure shows that the HFT can be considered as formed by two intersecting layers of variable thickness and width. Their cross-sections continuously transform along the HFT as follows

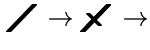

That is the width of the intersecting layers starts from a relatively large value (compared to the thickness) at one of the photospheric polarities, it grows further in the corona and shrinks abruptly to a small value at the other polarity, where it corresponds to the thickness of the other layer. Within one cross-section the thickness of the layers has in general a maximal value in the middle of the HFT and decreases monotonically towards the edges of the layers.

For $d \to 0$ the witdth of the layers is increasing while the thickness is continuously decreasing, so that for $d = 0$ they form two genuine separatrix surfaces intersecting along the separator field line (Figure 4). Thus the separatrix surfaces present in the $d = 0$ case

have to be considered as a result of a degenerated HFT.

Since the above layers collapse to the genuine separatrix surfaces in such a limiting transition, they should be identified with QSLs. This fits very well to our general definition of a QSL as a flux tube with $Q \gg 2$. Note, however, that such a flux tube has *the shape of a layer only in the major part of the volume*, while near one of the photospheric polarity the high width/thickness ratio decreases abruptly (see in Figure 8 the region of strong divergence of the field lines in the HFT). One can also conclude from the considered example that the magnetic surface $Q = \text{const} \gg 2$ may inclose not one but two QSLs simultaneously.

Finally, this example motivates also the following definition: *the quasi-separator is a field line of the HFT, on which Q attains a maximum.* The quasi-separator turns into the genuine separator when the corresponding null points appear at the photosphere or in the corona.

4.3. HFTs as a favourable site for magnetic reconnection

Although intersecting separatrix surfaces are the limiting case of an HFT, the topological argument on the current sheet formations along these surfaces and especially at the separator is no longer applicable to the HFT because of its topologically trivial structure. This does not exclude, however, that the quasi-separator plays a similar role in reconnection process as the genuine separator. It is simply necessary to find other arguments not based on magnetic topology. Below we propose two such arguments which rely only on geometrical and physical properties of the HFT.

First we have computed for our example the photospheric distribution of the differential flux volume V (25). This distribution demonstrates (Figure 10) that V has a very large gradient across the HFT-traces. According to *Schindler and Birn* [1999], this should be a sufficient condition for the development of current layers at the HFT during a general quasi-static evolution of the configuration.

However, quasi-static conditions may break down in the solar corona due to a special structure of the HFT. So it is worth to improve this approach by taking into account the dynamics. Notice first that the Jacobian $|\Delta|$ has mutually inverse values at the ends of a given field line. Therefore the corresponding areas of minimums and maximums of $|\Delta|$ are always connected to each other. Thus the $|\Delta|$-distribution identifies two pairs of short and long magnetic flux tubes whose projection on the photosphere are approximately traced in Figure 7b by dots and pluses. These tubes are actually a sort of ribs for the HFT as it is seen from Figures 8 and 9, where the boundary of the HFT and the $|\Delta|$-distribution are shown together. They are rooted with one end in the regions of strong magnetic field and therefore are qualitatively distinct structural elements of the configuration. Due to photospheric motion these tubes must somehow interact with each other in the HFT. The character of such an interaction can be appraised for the particular evolution in which the ideal plasma flow only 'shuffles' the field lines in configuration without temporal variation of the field itself. One can see from Figures 7b, 8 and 9 that such an evolution would have the following peculiarity: if a field line passes from one of the above mentioned tubes to another, so that one of its footpoints crosses slowly the narrow HFT-trace, then its other footpoint will sweep along the HFT-trace in the other polarity. Figures 5 and 7b also show that the HFT-traces connect the modelled sunspots, so that they serve as channels through which the field lines have an opportunity to switch from one sunspot to another, both of the same polarity. The aspect ratio of the HFT-traces in the considered example is of the order of $\sqrt{Q} \approx 10^3$. A crossing of the HFT-trace by a field line with a footpoint velocity $v \sim 1\,\mathrm{km/s}$ would require for its sweeping at the other end $v \sim 10^3\,\mathrm{km/s}$ – a value comparable with the Alfvén speed in the solar active regions. This demonstrates that the violation of the quasi-static conditions for such regions is reached foremost in HFTs, which in turn implies a current accumulation there and possible magnetic reconnection as well.

4.4. Observable manifestations

The transverse magnetic field in the middle part of the HFT has a pronounced hyperbolic structure (Figure 9), which is a characteristic feature of reconnection models [*Priest and Forbes,* 1992; *Hornig, G. and L. Rastätter,* 1998]. MHD simulations for the magnetic field with such a structure show a good correspondence between the locations of developing current layers and the QSLs determined by N [*Milano et al.* 1999]. This suggests that the favorable place for the development of a strong current layer and hence for the magnetic reconnection process is the middle part of the HFT. The energy released at this place is channelled to the photosphere by the corresponding

field lines to produce there brightenings in H_α-line. Therefore the HFT-traces can be identified with the H_α-ribbons of solar flares – a fact which *Gorbachev and Somov* [1988, 1989] explained by the presence of the separator in the configuration. From our approach, however, it is clear that for the configurations with the distributed photospheric field only the hyperbolic geometry has a real meaning, while the indicated separator is no more than an artefact originated by the auxiliary sub-photospheric point sources.

The flux tubes at the 'ribs' of the HFT contract towards the ends of the HFT-traces, which is reflected in the photospheric distribution of the Jacobian $|\Delta|$ as well as in the 3D structure of field lines (Figures 7 and 8). This suggests a natural explanation of the bright 'kernels' at the ends of flare ribbons: the contraction of the flux tubes at the ends of the HFT-traces has to concentrate the released energy in these regions and so to form such 'kernels'. *Gorbachev and Somov* [1989] came to the same conclusion, although their analysis of the global field line structure was erroneous. They claimed that the 'kernels' are connected to each other by field lines – this is impossible. As was shown above the contraction of the flux tubes at one end of the HFT is always accompanied by their expansion at the other end, otherwise the flux tubes in the HFT would not be squashed so much.

The degree of squashing depends on how the magnetic flux is distributed on the photosphere. It must be higher for the configurations with well concentrated sources and lower in the opposite case. Due to this dependence, the H_α-brightenings of flares have to be stronger in the 'kernels' or ribbons, respectively. This property of magnetic connectivity naturally explains the observed morphological difference between compact and two-ribbon flares.

Thus, we have demonstrated in the simplest potential approximation that the existence of the ribbons is due to the special geometrical structure of the HFT. Moreover, the previous investigations based both on the norm N [*Démoulin et al.,* 1996] and on the squashing degree Q [*Titov et al.,* 1999] suggest that non-potential magnetic configurations have similar properties.

4.5. The orthogonal parquet in a quadrupole configuration

The distributions of Q and $|\Delta|$ yield the most important but not the full information about the magnetic connectivity in a given configuration. In particular Q and $|\Delta|$ do not show how the elemental flux tubes are arranged around the HFT to provide its continuous embedding in the whole quadrupole configuration. This information can be obtained by computing the orthogonal parquet according to the above formulated theory. The result for the example from Figure 5 is shown in Figure 11.

The resulting pattern of orthogonal $\mathbf{u}$- and $\mathbf{v}$-field lines (called also λ_1- and λ_2-lines) has several critical points where the $(\mathbf{u}, \mathbf{v})$-pair is not uniquely determined. These are three pairs of I-points and two pairs of Y-points. Due to the mapping of field lines from the region of positive to the region of negative polarity each critical point has its counterpart in the other polarity, denoted by upper indices $+$ or $-$, depending on the polarity they locate in.

The separatrix λ-lines emanating from critical points devide the plane in several regions, each of which has its counterpart in the opposite polarity. The corresponding regions are shaded in the same grey halftones and for the corresponding separatrices the same line style is used, so that dashed (solid) lines are mapped onto dashed (solid) ones. As was shown in Section 3.4, a pair of separatrix λ_1- and λ_2-lines emanates from an I-point in opposite directions to meet the other I-point (see the points $I_2^\pm$ and $I_3^\pm$ in Figure 11) or to intersect the other separatrice (see the points $I_1^\pm$ and $I_3^\pm$). For Y-points there are alltogether six separatrices, three of both types. They intersect other separatrices or the polarity inversion line to divide the whole plane on several domains with a simple orthogonal parquet inside. To reduce the number of such domains, each separatrice has been terminated just after the first intersection with the other.

One can see from Figure 11 that the devision of the photospheric plane in such domains is in itself rather involved. To avoid an excessive complexity of the figure, the λ-lines of the parquet are reproduced only in the most interesting domains, i.e. those which inclose the HFT-traces. In these domains the Q-distribution presented earlier in Figure 7a is shown as well to indicate the exact location of the HFT-traces. Everywhere else crosses indicate the directions of the vectors $\mathbf{u}$ and $\mathbf{v}$. The λ-lines mapped onto each other are shown in different polarities in the same style. This helps to see that the long λ-lines parallel to the HFT-traces are mapped to the short λ-lines perpendicular to the HFT-traces – exactly as it follows from the above discussed $|\Delta|$-distribution.

Comparing pairs of appropriate domains, one can clearly see how the combination of stretching, contraction and expansion of the flux tubes around the

HFT provides a continuous transition from this geometrically complex object to a more simple surrounding field structure. Thus the described technique is rather helpful for analysing magnetic configurations.

4.6. Concentrated versus distributed sources

A careful investigation of magnetic connectivity as described above is a rather laborious matter. So it is useful to have a simpler method for an 'express analysis' of the coronal field structure. The point source model provides such a method for the case, where a magnetogram under study has well pronounced extremums of the vertical magnetic field. In this case one can aggregate magnetic flux nearby these extremums in the corresponding photospheric point sources and investigate the structure of the field produced by these sources. As a matter of fact such a simplified configuration has a non-trivial magnetic topology due the presence of several null points. Most of the nulls, however, will be located on the photosphere and so they will disappear in a more accurate model with a distributed photospheric field as it is clear from the previously considered example. The remaining nulls may shift to the corona, while some of the dissappearing nulls give birth to bald patches, thereby determining the topological skeleton of the configuration [*Bungey et al.,* 1996]. The rest of the nulls disappearing in this transition from one model to the other give actually rise to geometrical features. In particular, if a pair of the disappearing nulls belongs to a separator as in our example, it will produce an HFT. The separatrix spine lines and fan surfaces of the nulls (in more detail about spines and fans see [*Priest and Titov,* 1996]) helps here to anticipate the structure of the HFT in the model with distributed magnetic flux. Our example shows that the HFT-traces are approximately located *along the spine lines* of the source model – these are the separatrix lines approaching the nulls perpendicularly to the fan surfaces (cf. Figures 4–8). The fan surfaces themselves do not leave features at the places, where such a disappearance of the nulls occur. Only with these reservations the source models may be useful for investigating the structure of the coronal magnetic field.

5. Conclusions

We have shown that the complete description of the magnetic connectivity is given by the four metrical quantities invariant with respect to the direction of the field line mapping. Two of them are squashing and contraction-expansion degrees of the elemental magnetic flux tubes. The second pair of quantities determine the directions of the corresponding dilations of the tubes on the photosphere. All four characteristics can be combined in one geometrical object called orthogonal parquet. This is a global photospheric network with curvilinear rectangular cells representing the cross-sections of the respective flux tubes at their ends.

The singularities and discontinuities in the photospheric distributions of the first two values correspond to the topological features of the coronal field. They reveal the genuine separatrix surfaces associated with magnetic nulls and bald patches. The topologically trivial regions are characterised by smooth distributions of the above values. Nevertheless, they may contain geometrical features, namely the strongly squashed flux tubes called quasi-separatrix layers (QSLs).

The considered example of the topologically simple quadrupole configuration has illustrated this approach 'in action' by demonstrating its high efficiency in analysing the structure of coronal magnetic fields. We have shown that this configuration may have a geometrical feature called hyperbolic flux tube (HFT), which is a special combination of two QSLs. The theoretical and observational arguments are given in support of the HFT as a favourable site for magnetic reconnection in solar flares.

The geometrical and topological properties of magnetic connectivity, that is those which are based on the metric or are independent of it, are often confused in astrophysics. This is a source of misleading concepts and results rather than only a question of terminology. In our approach the borderline between the geometrical and topological descriptions is clearly defined, which helps to see an urgent need in revising the present mechanisms of current sheet formation in the solar corona.

Acknowledgment. We are grateful to one of the referees for the useful comments. We thankfully acknowledge financial support from the Volkswagen-Foundation and the grant of the British-German Research Collaboration.

References

Baum, P. J. and A. Bratenahl, Flux linkages of bipolar sunspot groups – A computer study *Solar Phys., 67*, 245–258, 1980.

Bungey, T. N., V. S. Titov, and E. R. Priest, Basic topological elements of coronal magnetic fields, *Astron. As-*

trophys., 308, 233–247, 1996.

Démoulin, P., E. R. Priest and D. P. Lonie, 3D magnetic reconnection without null points 2. Application to twisted flux tubes, *J. Geophys. Res., 101* , 7631–7646, 1996.

Démoulin, P., L. G. Bagalá, C. H. Mandrini, J. C. Hénoux and M. G. Rovira, Quasi-separatrix layers in solar flares. II. Observed magnetic configurations, *Astron. Astrophys., 325*, 305–317, 1997.

Gorbachev, V. S. and B. V. Somov, Photospheric vortex flows as a cause for two-ribbon flares: a topological model, *Solar Phys., 117*, 77–88, 1988.

Gorbachev, V. S. and B. V. Somov, Solar flares of November 5, 1980, as the result of magnetic reconnection at a separator, *Soviet Astronomy–AJ 33*, 57–61, 1989.

Hornig, G. and L. Rastätter, The magnetic structure of $\mathbf{B} \neq \mathbf{0}$-reconnection, *Physica Scripta T74*, 34–39, 1998.

Inverarity, G. W., and V. S. Titov, Formation of current layers in three-dimensional inhomogeneous coronal magnetic fields by photospheric motions, *J. Geophys. Res., 102*, 22285–22293, 1997.

Kippenhahn, R., and A. Schlüter, Eine Theorie der solaren Filamente, *Z. Astrophys., 43*, 36–62, 1957.

Lau, Y.-T, Magnetic nulls and topology in a class of solar flare models, *Solar Phys., 148*, 301–324, 1993.

Longcope, D. W., and H. R. Strauss, The form of ideal current layers in line-tied magnetic fields, *Astrophys. J., 437*, 851–859, 1994.

Low, B. C., and R. Wolfson, Spontaneous formation of electric current sheets and the origin of solar flares, *Astrophys. J., 324*, 574–581, 1988.

Mandrini, C. H., P. Démoulin, M. G. Rovira, J.-F. de La Beaujardiere and J. C Hénoux, Constraints on flare models set by the active region magnetic topology. Magnetic topology of AR 6233, *Astron. Astrophys., 303*, 927–939, 1995.

Milano, L. J., P. Dmitruk, C. H. Mandrini, D. O. Gómez, P. Démoulin, Quasi-separatrix layers in a reduced magnetohydrodynamic model of a coronal loop, *Astrophys. J., 521*, 889–897, 1999.

Priest, E. R., and P. Démoulin, Three-dimensional magnetic reconnection without null points 1. Basic theory of magnetic flipping, *J. Geophys. Res., 100*, 23443–23463, 1995.

Priest, E. R., and T. G. Forbes, Magnetic flipping: reconnection in three dimensions without null points, *J. Geophys. Res., 97*, 1521–1531, 1992.

Priest, E. R., and V. S. Titov, Magnetic reconnection at three-dimensional null points, *Phil. Trans. R. Soc. Lond. A, 354*, 2951–2992, 1996.

Schindler, K., and J. Birn, Thin current sheets and magnetotail dynamics, *J. Geophys. Res., 104*, 25001-25010, 1999.

Seehafer, N., On the magnetic field line topology in solar active regions, *Solar Phys., 105*, 223–235, 1986.

Sweet, P. A., Mechanisms of solar flares, *ARA&A, 7*, 149–177, 1969.

Titov, V. S., Topology and reconnection of magnetic fields in the solar corona (in Russian), *Izv. Akad. Nauk, Ser. fiz., 63*, 1497-1511, 1999.

Titov, V. S., and G. Hornig, Magnetic connectivity of coronal fields: geometrical versus topological description, 33rd COSPAR Scientific Assembly, *Adv. Space Res.*, 2002, in press.

Titov, V. S., P. Démoulin and G. Hornig, Quasi-separatrix layers: refined theory and its application to solar flares, in *Magnetic fields and solar processes*, 9-th European Meeting on Solar Physics, ESA SP-448, edited by A. Wilson, pp. 715-722, ESA Publications Division ESTEC, Noordwijk, The Netherlands, 1999.

Titov, V. S., E. R. Priest and P. Démoulin, Conditions for the appearance of "bald patches" at the solar surface, *Astron. Astrophys., 276*, 564–570, 1993.

Vekstein, G. E., and E. R. Priest, Magnetohydrodynamic equilibria and cusp formation at an X-type neutral line by footpoint shearing, *Astrophys. J., 384*, 333–340, 1992.

Vekstein, G. E., E. R. Priest and T. Amari, Formation of current sheets in force-free magnetic fields, *Astron. Astrophys., 243*, 492–500, 1991.

Zwingmann, W., K. Schindler and J. Birn, On sheared magnetic-field structures containing neutral points, *Solar Phys., 99*, 133–143, 1985.

G. Hornig and V.S. Titov, Theoretische Physik IV, Fakultät für Physik und Astronomie, Ruhr-Universität Bochum, 44780 Bochum, Germany. (e-mail: gh@tp4.ruhr-uni-bochum.de; st@tp4.ruhr-uni-bochum.de)

P. Démoulin, DASOP, Observatoire de Paris-Meudon, F 92195 Meudon cedex, France (e-mail: Pascal.Demoulin@obsp

Received , 2001

This preprint was prepared with AGU's LaTeX macros v5.01. File mgncon3˙ formatted February 27, 2002.

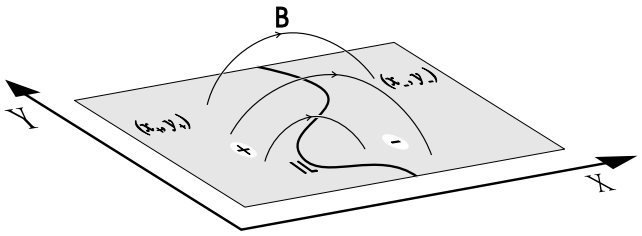

Figure 1. The photospheric plane and magnetic field lines connecting positive and negative polarities, which are separated by the inversion line (IL).

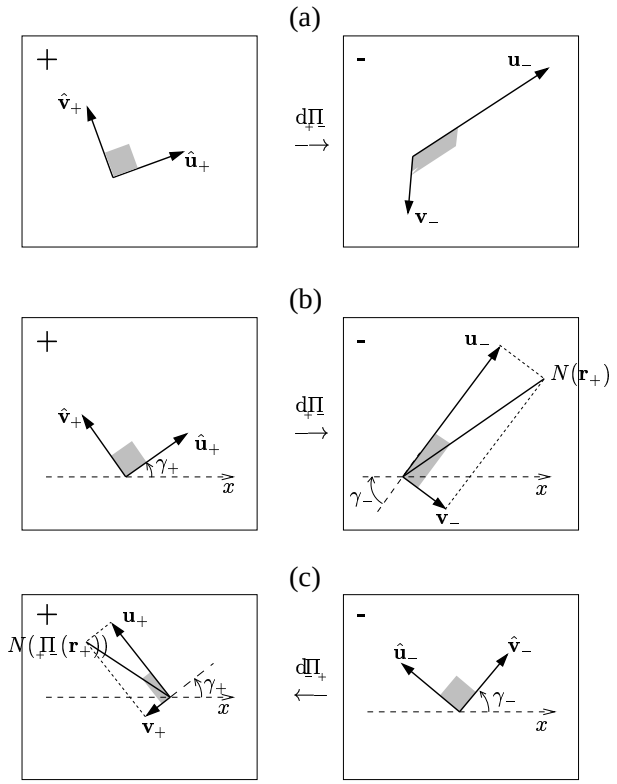

Figure 2. The mapping of an orthonormal basis $(\hat{\mathbf{u}}_+, \hat{\mathbf{v}}_+)$ by the differential $\mathrm{d}\underset{+}{\underline{\Pi}}$ (a,b): the basis $(\mathbf{u}_-, \mathbf{v}_-)$ is in general non-orthonormal (a), but it is orthogonal for a special orientation of $(\hat{\mathbf{u}}_+, \hat{\mathbf{v}}_+)$ (b) when $|\mathbf{u}_- + \mathbf{v}_-|$ determines the norm $N(\mathbf{r}_+)$. The inverse differential $\mathrm{d}\underset{-}{\underline{\Pi}}_+$ maps the orthonormal basis $(\hat{\mathbf{u}}_-, \hat{\mathbf{v}}_-)$, rotated with respect to $(\mathbf{u}_-, \mathbf{v}_-)$ on $\pi/2$, into the orthogonal basis $(\mathbf{u}_+, \mathbf{v}_+)$ (c), so that $|\mathbf{u}_+|/|\mathbf{v}_+| = |\mathbf{u}_-|/|\mathbf{v}_-|$ but $|\mathbf{u}_+ + \mathbf{v}_+| = N(\underset{+}{\underline{\Pi}}(\mathbf{r}_+)) \neq N(\mathbf{r}_+)$. The shaded areas show how these properties of the mappings manifest in the corresponding cross-sections of thin flux tubes.

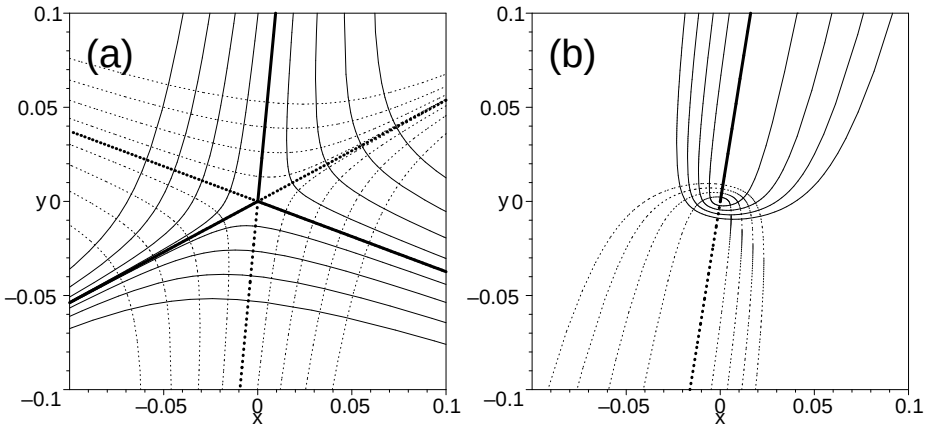

Figure 3. The local structure of λ_1- (solid) and λ_2-lines (dashed) in the vicinity of critical points of Y- (a) and I-types (b) (see Section 3.5). The thick lines represent the corresponding separatrices.

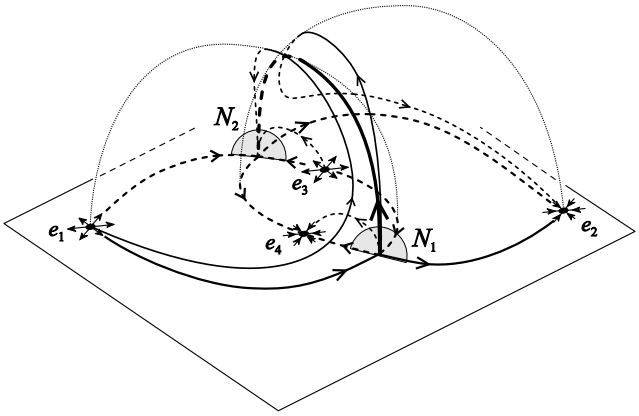

Figure 4. The separator in the configuration with four point-like sources is a field line (the thickest solid line) connecting two nulls N_1 and N_2 (cf. Figure 10 in [*Sweet*, 1969]). The light grey semicircles represent the separatrix fan surfaces near these nulls; the separatrix spine lines are perpendicular to the fans.

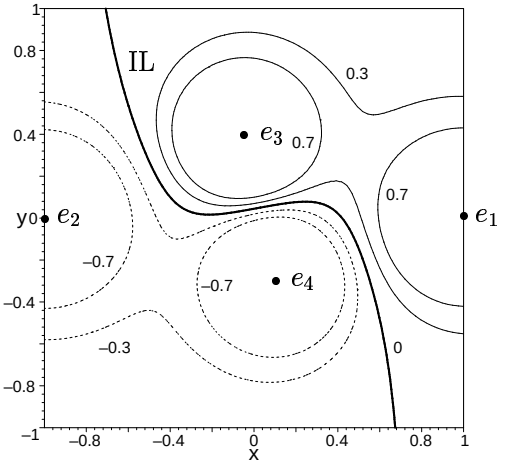

Figure 5. The photospheric distribution of the vertical magnetic field for the point sources $e_1 = -e_2 = 0.6$ and $e_3 = -e_4 = 0.4$ placed below the photosphere ($z = 0$) on the plane $z = -0.1$ (cf. Figure 1c in [*Gorbachev and Somov*,1988]). The IL is a thick solid line.

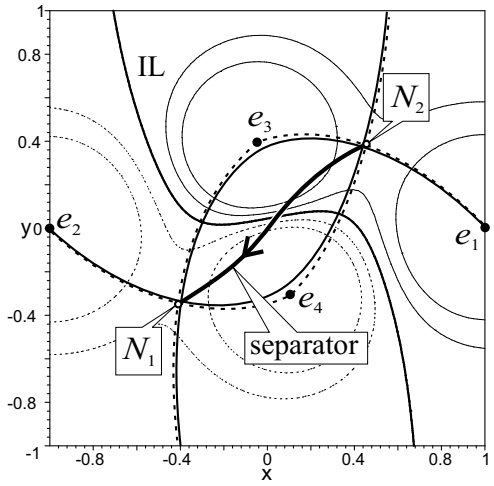

Figure 6. The separator in the model of *Gorbachev and Somov* [1988]. The dashed lines passing through the fictive charges and nulls N_1 and N_2 are intersections of the fictive separatrix surfaces with the plane of the charges, while the neighboring solid lines are the corresponding intersections with the photosphere.

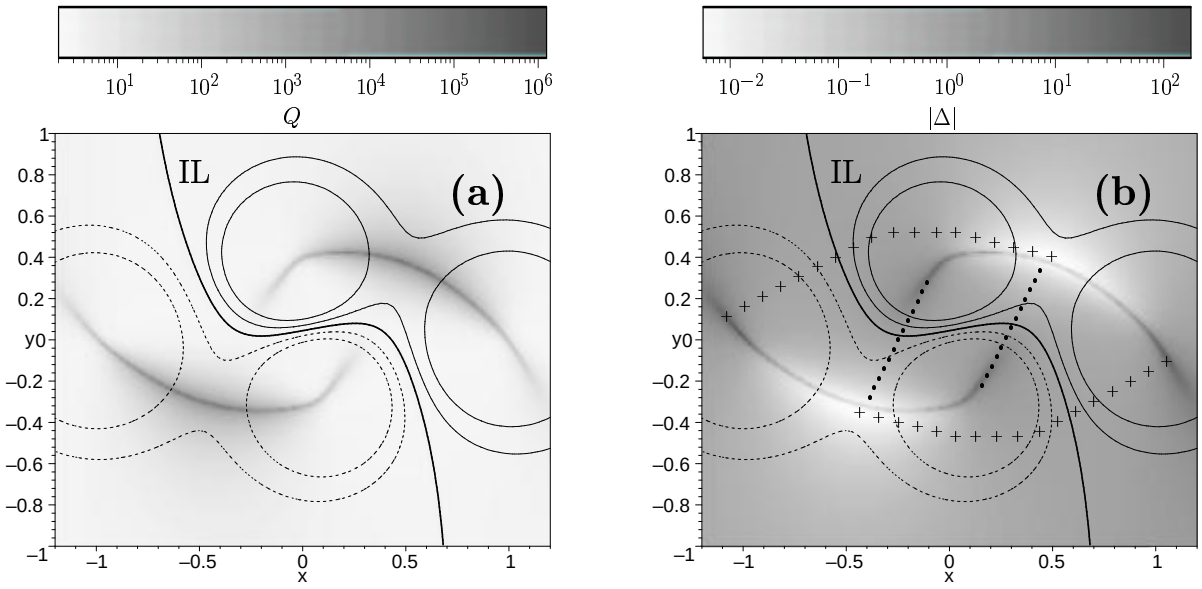

Figure 7. The photospheric distributions of Q (a) and $|\Delta|$ (b) superimposed with the corresponding magnetogram (Figure 5); the dots and pluses trace the vertical projection of the four interacting flux tubes on the photosphere.

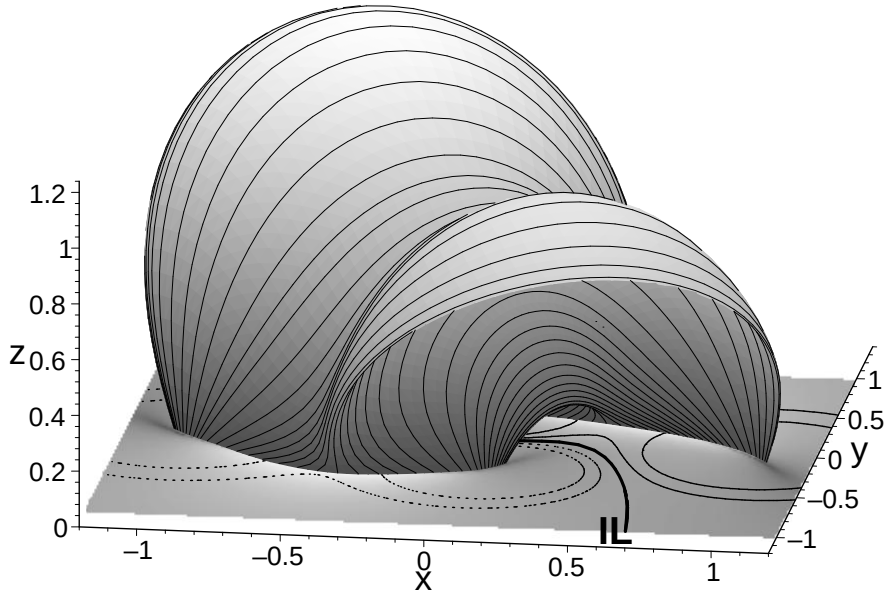

Figure 8. The magnetic flux surface $Q = 100$ enclosing the hyperbolic flux tube. In the photospheric plane $z = 0$ the distribution of $|\Delta|$ is shown superimposed with the same magnetogram is shown as in Figure 7b

.

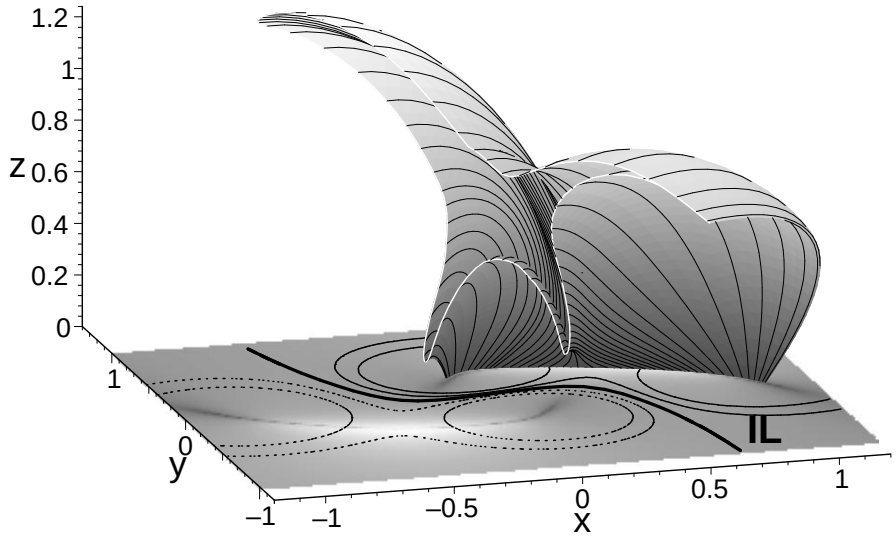

Figure 9. The half of magnetic flux surface $Q = 100$ enclosing the hyperbolic flux tube. The cross-section is made at the half-length of the field lines belonging to this surface. In the photospheric plane $z = 0$ the distribution of $|\Delta|$ is shown superimposed with the magnetogram from Figure 7b.

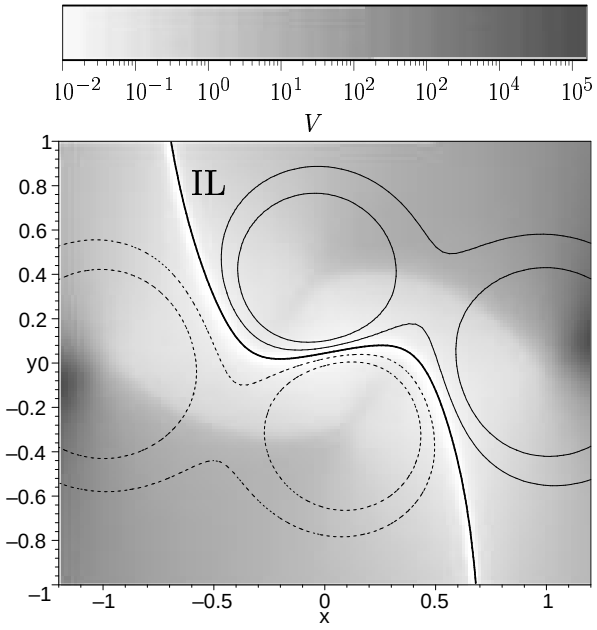

Figure 10. The photospheric distribution of differential flux volume V superimposed with the corresponding magnetogram (Figure 5).

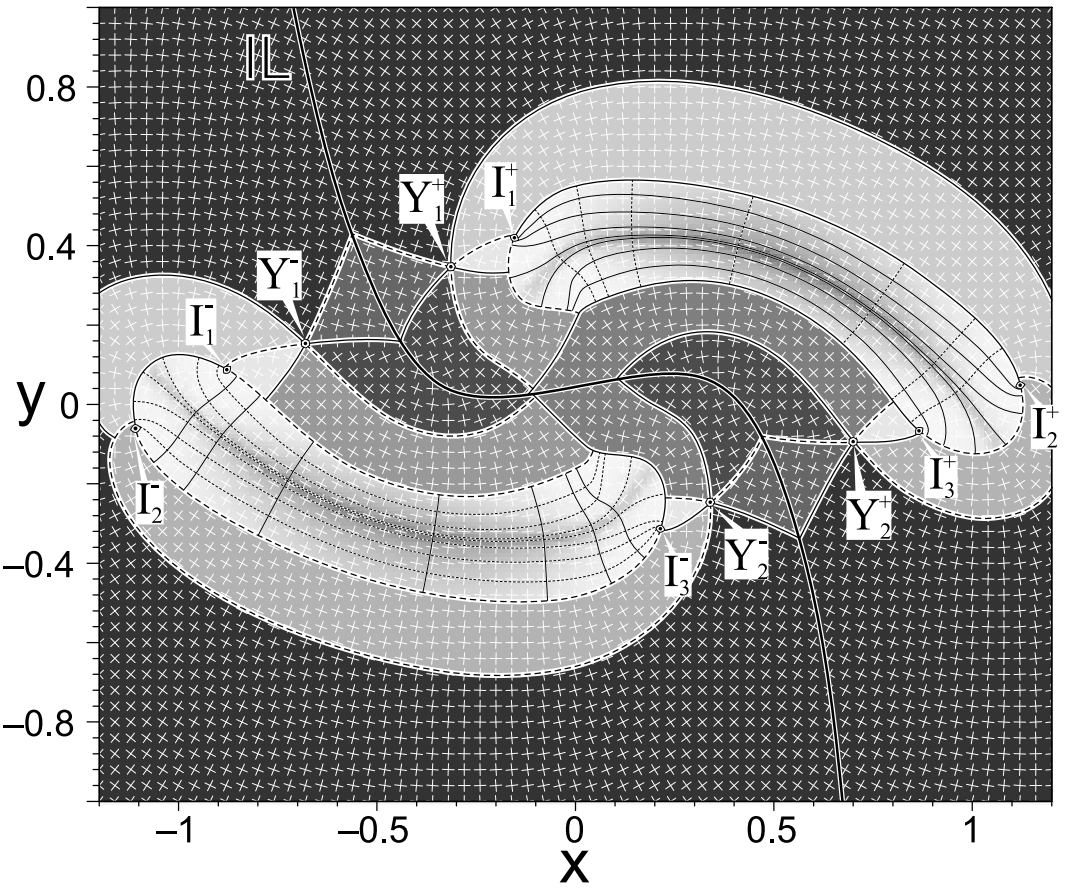

Figure 11. The devison of the photospheric plane in domains of a simple orthogonal parquet for the configuration from Figure 5 by λ-lines emanating from the critical Y- and I-points (see Figure 3 and Sections 3.4 and 4.5). The linked domains are shaded in the same grey halftones. The λ_1-lines are dashed in the positive polarity and mapped onto dashed λ_2-lines in the negative polarity, and vice versa for the solid λ-lines. λ-lines of the orthogonal parquet are plotted in the domains enclosing the HFT-traces. The separatrix λ-lines are shown of larger thickness than the normal ones. The crosses represent the directions of the corresponding **u**- and **v**-fields.